iScience

CellPress

Article

Bioinspired Anti-digestive Hydrogels Selected by a Simulated Gut Microfluidic Chip for Closing Gastrointestinal Fistula

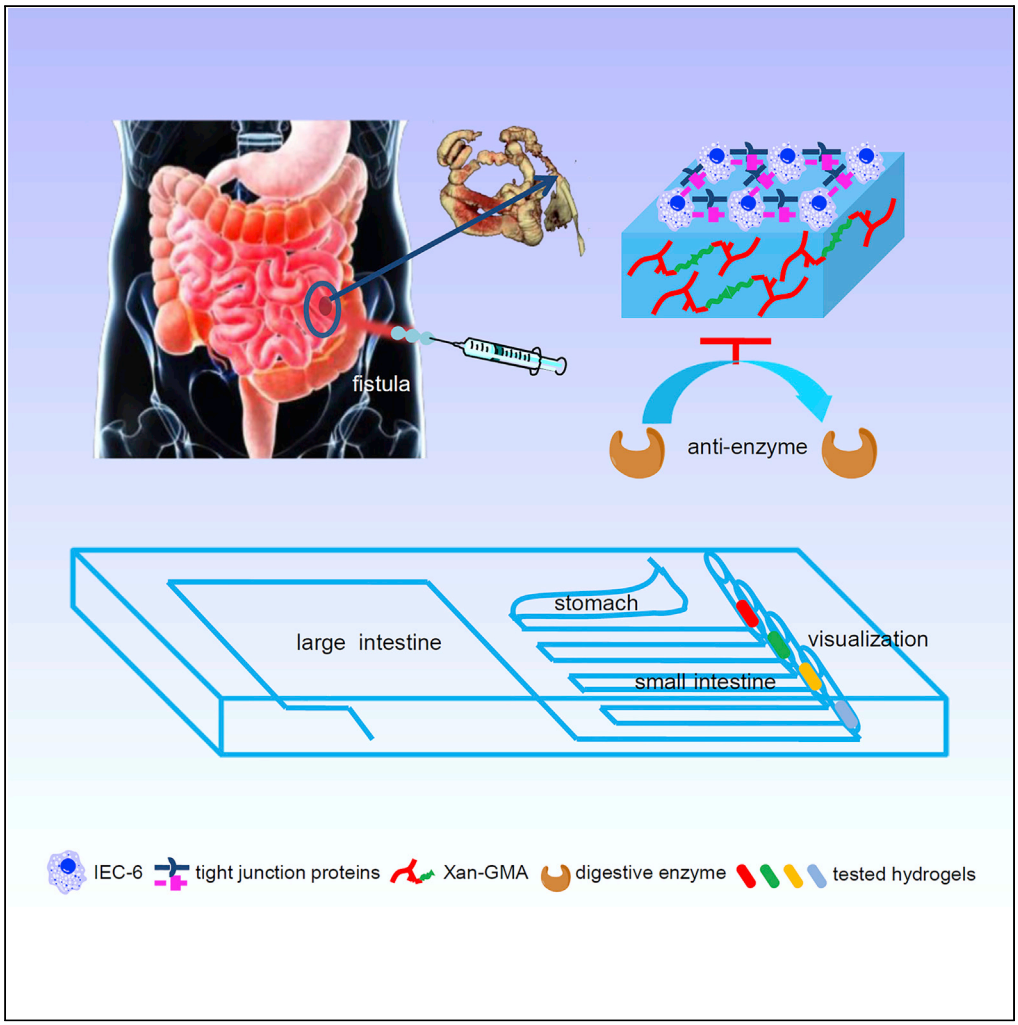

Jinjian Huang, Zongan Li, Qiongyuan Hu, Guopu Chen, Yanhan Ren, Xiuwen Wu, Jianan Ren

jiananr@gmail.com

HIGHLIGHTS

Xanthan-based injectable hydrogel was inspired by indigestibility of dietary fibers

The hydrogel restored the gut barrier functions of IEC-6 cells

The hydrogel was verified to be anti-digestive by a simulated gut microfluidic chip

The hydrogel may achieve a better effect in closing GI fistula than fibrin sealant

Huang et al., iScience 8, 40–48
October 26, 2018
https://doi.org/10.1016/j.isci.2018.09.011

iScience

CellPress

Article

Bioinspired Anti-digestive Hydrogels Selected by a Simulated Gut Microfluidic Chip for Closing Gastrointestinal Fistula

Jinjian Huang,[1,2] Zongan Li,[3] Qiongyuan Hu,[2] Guopu Chen,[2] Yanhan Ren,[4] Xiuwen Wu,[2] and Jianan Ren[1,2,5,*]

SUMMARY

The anti-digestive features given to hydrogels can prolong their action time in gut environment; however, these types of hydrogels have rarely been reported. Inspired by indigestibility of dietary fibers, we introduced an injectable covalent hydrogel through photopolymerization of glycidyl methacrylate-modified xanthan. This newly synthesized hydrogel exhibited a specific concentration-dependent porosity, swelling ratio, and stiffness. The intestinal epithelial cells-6 could grow on the surface of the stiffer hydrogel, and achieved their gut barrier functions. A simulated gut microfluidic chip was manufactured to demonstrate the hydrogel's good performance of anti-digestion compared with the current product, fibrin sealant. Furthermore, calcium ions could induce the swelling-shrinking behavior of the hydrogel, which assisted in removing the hydrogels at the proper time so as to avoid the mismatch of hydrogel degradation and tissue regeneration. Therefore, this hydrogel is expected to be an outstanding gut repair material, especially for closing gastrointestinal fistula.

INTRODUCTION

Anti-digestive biomaterials have tremendous promising application potentials in the alimentary system, such as oral drug delivery and gut bioengineering (Bitar and Zakhem, 2016). For example, pH-responsive microparticles can deliver therapeutic drugs to the small intestine, but unfortunately they are degraded within 1 h, showing neither clear effects of sustained release (Koetting et al., 2016) nor colon-targeted release (Xiao et al., 2016). Moreover, the gut differs from other human systems owing to the presence of digestive enzymes, which pose challenges to tissue scaffolds (Bitar et al., 2014). Therefore, priority should be given to the development of biocompatible anti-digestive materials.

Inspired by the resistance of dietary fibers to digestion and absorption in digestive tract (Korcz et al., 2018), xanthan is regarded as an excellent candidate to generate such materials. The anti-digestive performance of xanthan is largely associated with its specific structure (Kumar et al., 2018). First, the backbone of xanthan is similar to that of cellulose, preventing its breakdown by common cellulases. Second, its trisaccharide side chains are likely to act as a barrier to enzymatic attack. Last, xanthan has the secondary structure of ordered double-stranded helix (Holzwarth and Prestridge, 1977), which increases its tolerance to enzymolysis.

In addition, xanthan is a type of natural polysaccharides, thus exhibiting excellent biocompatibility (de Vos et al., 2014). *In vitro* experiments have found that fibroblasts can survive well on the surface of xanthan-based scaffolds (Bueno et al., 2015; Elizalde-Pena et al., 2013). *In vivo* studies have demonstrated that foreign body reactions induced by multinuclear giant cells are mild after subcutaneous injection of xanthan-based hydrogels (Huang et al., 2018). However, the effects of xanthan-based materials on gut barrier functions remain unclear.

Gastrointestinal (GI) fistula is manifested through the destruction of GI continuity and damage to the gut barrier. It is the most feared complication after abdominal surgery and carries a mortality rate of 5%–30% (Altomare et al., 1990; Campos et al., 1999). An animal model of GI fistula has not been constructed so far, leading to great limitations in developing materials for fistula repair. Recent progress in the closure of GI fistula has focused on the fibrin sealant, which can achieve fistular healing within 3–8 days (Wu et al., 2014). However, the fibrin sealant can only exist in the digestive juice for less than 12 hr (Huang et al., 2018), which is far below the desired duration. Therefore, injectable anti-digestive hydrogels may have an advantage over the fibrin sealant because they have more sustained effects.

[1]School of Medicine, Southeast University, Nanjing, China

[2]Lab for Trauma and Surgical Infections, Department of Surgery, Jinling Hospital, 305 East Zhongshan Road, Nanjing 210002, China

[3]NARI School of Electrical and Automation Engineering, Nanjing Normal University, Nanjing, China

[4]Chicago Medical School, Rosalind Franklin University of Medicine and Science, North Chicago, IL, USA

[5]Lead Contact

*Correspondence: jiananr@gmail.com

https://doi.org/10.1016/j.isci.2018.09.011

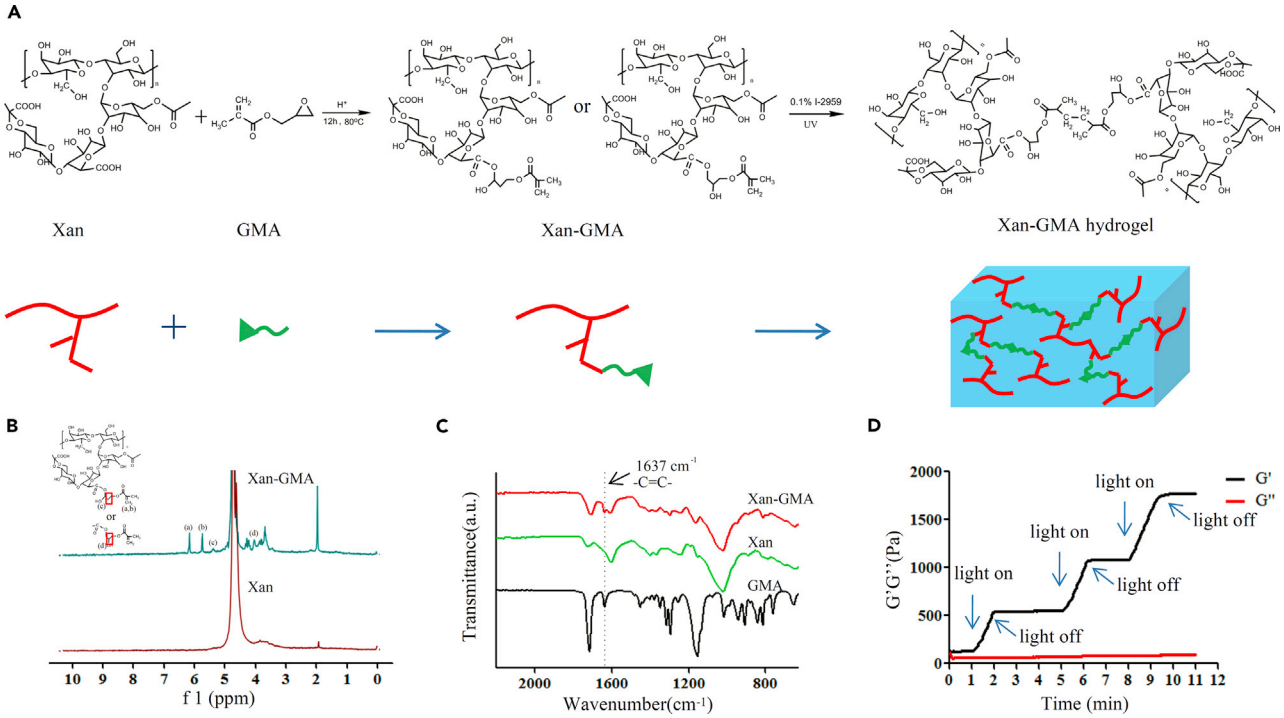

Figure 1. Characterization of xan-GMA and xan-GMA Hydrogels

(A) Flow chart to synthesize xan-GMA and xan-GMA hydrogels.

(B) ^{1}H-NMR spectrum, a = 6.17, b = 5.76, c = 5.06, and d = 4.02; the magnified version can be found in Figure S2.

(C) Fourier transform infrared spectrum; the magnified version can be found in Figure S3.

(D) Rheological changes of 10% xan-GMA solution during the three on and off cycles of UV light.

Based on the aforementioned findings, we reported an injectable anti-digestive hydrogel through photopolymerization of glycidyl methacrylate (GMA)-modified xanthan. The GMA-conjugated xanthan (xan-GMA) was gelated upon UV light exposure. We investigated the changes in porosity, swelling ratio, and stiffness of xan-GMA hydrogels, along with the effects of these changes on IEC-6 cells. A simulated gut microfluidic chip was used to compare the anti-digestive ability of xan-GMA hydrogel with that of the fibrin sealant. Moreover, calcium ions were used to trigger hydrogel shrinkage, which could then be removed timeously. Our results promote the clinical translation of xan-GMA hydrogels for closing GI fistula.

RESULTS AND DISCUSSION

Successful Synthesis of xan-GMA and xan-GMA Hydrogels

xan-GMA was prepared through the transesterification reaction between xanthan and GMA (Figure 1A). The molar ratio of GMA to carboxyl groups in xanthan was 4:1, and the substitution degree of GMA was 10%. The chemical structure of the product was examined by ^{1}H-nuclear magnetic resonance (NMR) spectroscopy (Figure 1B). The ^{1}H-NMR spectrum of xanthan was similar to that reported previously (Kumar et al., 2017; Makhado et al., 2017). For xan-GMA, the signals at δ = 5.76 and 6.17 referred to the vinyl protons, which suggested the presence of GMA on xanthan. This reaction generated two products as isomers: 3-methacryloyl-1-glyceryl and 3-methacryloyl-2-glyceryl esters, and the signals at δ = 5.06 and 4.02 belonged to the hydrogen of the methacryloyl-1-glyceryl and methacryloyl-2-glyceryl esters, respectively (Reis et al., 2009). However, it was hard to calculate their relative ratio due to the overlap of corresponding peaks with those of other protons. Furthermore, the Fourier transform infrared spectra of the product also confirmed the successful conjugation of GMA onto xanthan (Figure 1C), since the C=C groups of GMA clearly appeared at the absorption of 1,637cm^{-1}.

The xan-GMA hydrogels were gelated by photopolymerization. It was inferred by rheology that storage modulus G′ would increase upon UV light exposure, whereas the value would be constant after withdrawal

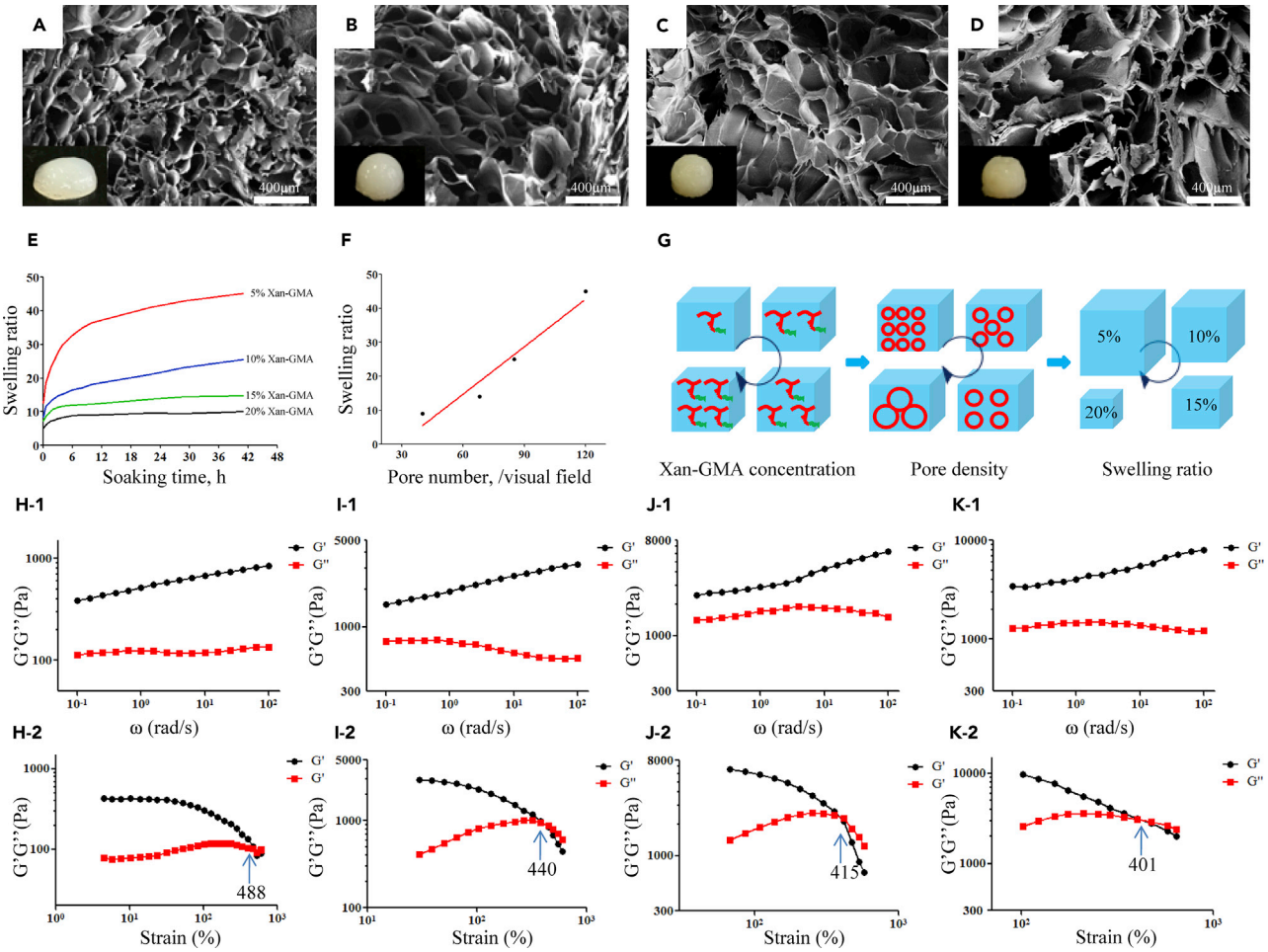

Figure 2. Physical Properties of xan-GMA Hydrogels

(A–D) Microstructure of the hydrogels with different concentrations of xan-GMA at (A) 5%, (B) 10%, (C) 15%, and (D) 20%. The embedded pictures at the left bottom represent the real products.

(E) Swelling ratio.

(F) Relations of pore density and swelling ratio.

(G) Schematic diagram illustrating the relations of xan-GMA concentration, pore density, and swelling ratio.

(H–K) Rheological results of hydrogels with different xan-GMA concentrations of (H-1 and H-2) 5%, (I-1 and I-2) 10%, (J-1 and J-2) 15%, and (K-1 and K-2) 20% (1, frequency sweep; 2, strain sweep).

of the light source (Figure 1D). Owing to the presence of xan-GMA isomers, the products had three combinations after gelation (Figure S1).

Physical Properties of xan-GMA Hydrogels and Their Effects on IEC-6 Cells

Similar to other hydrogels, xan-GMA hydrogels exhibited three-dimensional porous structure (Figures 2A–2D), which was considered an important architecture to conduct gas and water exchanges for biological systems (Ghobril and Grinstaff, 2015). With the rising concentration of xan-GMA, the average pore size increased, and accordingly, the pore density decreased. It indicated that the degree of cross-linking of xan-GMA decreased as the concentration increased. This negative correlation was probably attributed to the steric hindrance that resulted from the high concentration of xan-GMA, which hindered the C=C groups from participating in the photopolymerization reaction. The swelling ratio was increased as the concentration of xan-GMA decreased (Figure 2E), and a positive linear relation was present between the swelling ratio and pore density (Figure 2F). This finding indicated that the quantity of pores inside the hydrogels was responsible for their swelling abilities (Figure 2G).

The concentration of xan-GMA altered the mechanics of the hydrogels. The storage modulus G′ and loss modulus G″ increased with the increase of xan-GMA concentration (Figures 2H-1–2K-1). The G′ of the 20% xan-GMA hydrogel (~10,000 Pa) was almost 10 times that of the 5% xan-GMA hydrogel (~1000 Pa) at 100 rad/s, and G′ increased as the angular frequency (ω) increased. This suggested that the intermolecular interactions of hydrogen bonds were enhanced when the xan-GMA concentration increased but were disrupted after application of external high-frequency oscillating forces (Li et al., 2012). In the oscillatory strain sweep experiment, the gel-sol transition point represented the start of the collapse of the gel network structure into a quasi-liquid (Liu et al., 2017). This experiment demonstrated that hydrogels with different concentrations of xan-GMA had similar resistance competence to the oscillation strain (~400%–500%) (Figures 2H-2–2K-2).

The variation in the physical properties of hydrogels may have an impact on cell behavior. For example, the fates of neural stem cells (NSCs) may be regulated by the stiffness of biomaterials. NSCs do not survive well in extremely soft (<0.1 kPa) or extremely hard (>100 kPa) materials, but they are prone to neuronal differentiation at a stiffness of 0.1–1 kPa and glial differentiation at a stiffness of 7–10 kPa (Tseng et al., 2015). The morphology of fibroblasts is also influenced by stiffness. Stiffness less than 5 kPa can lead to an abnormal morphology (circular) of fibroblasts, whereas they can show a normal morphology (elongated and spread) if the value is more than 20 kPa (Motealleh and Kehr, 2017). However, the effect on enterocytes was unclear. Therefore, we investigated this topic from aspects of cellular function and proliferation of IEC-6 cells. TJ proteins, ZO-1 and occludin, are fundamental molecules to prevent the invasion of gut bacteria and restore gut homeostasis (Cruz-Acuna et al., 2017). Through immunofluorescent staining (Figure 3A), we found that IEC-6 cells expressed ZO-1 and occludin proteins after culture on the surface of fibrin sealant and xan-GMA hydrogels for 3 days. The fluorescence intensity was comparable between the fibrin sealant and all groups of xan-GMA hydrogels, except the 5% xan-GMA hydrogel (Figure S4). The 3-(4,5-dimethylthiazol-2-yl)-2,5-diphenyltetrazolium bromide (MTT) assay further revealed that the proliferation capacity was significantly reduced after culture on the 5% xan-GMA hydrogel for 3 days (Figure 3B). Moreover, the 5% xan-GMA hydrogels presented a smaller pore diameter (Figure 2A), which might add to the difficulties for cells to exchange nutrients and water with the outer environment. Together, these results indicated that IEC-6 cells preferred to grow on the stiffer hydrogels with megapores (Figure 3C) (Staruch et al., 2017) and showed the non-inferiority of xan-GMA hydrogels to the commercial fibrin sealant at the cellular level if the xan-GMA concentration was more than 10%. Therefore, the xan-GMA hydrogels had demonstrated promising potentials in closing GI fistula and repairing gut barrier through the "bridging" effects (Figure 3D).

Measurement of Anti-digestive Activity by a Simulated Gut Microfluidic Chip

The alimentary system is a complicated system featured by the presence of various digestive enzymes, which can lead to the irritation of surrounding tissues after the formation of GI fistula and a consequent delay in its healing (Huang et al., 2017). Owing to the lack of animal models of GI fistula, we constructed a microfluidic chip that mimicked the anatomy of GI fistula with consistent irrigation by human intestinal juice (Figures 4A and 4B). This chip was used as an eligible replacement of GI fistula models to detect the anti-digestive performance. The advantages of this method were its simplicity, accuracy, visualization, and feasibility in laboratory settings.

The flow channel for digestive juice was 200 μm in diameter (Figures 4C–4E). Four opening holes (100 μm in diameter) located at the position of the "small intestine" were designed as the "fistula sites." The entire equipment consisted of the syringe pump, thin plastic pipes, microfluidic chip, glass capillaries, and beaker. The tested hydrogels were gelated in the glass capillaries in advance and then inserted at the "fistula sites." Digestion of the hydrogels was constantly observed using this microdevice. We found that more than half of the length of the fibrin sealant was degraded at 6 hr and completely degraded within 12 hr. In contrast, only a small amount of xan-GMA hydrogels was digested at 3 days (Figures 4F–4H). Therefore, it was concluded that the xan-GMA hydrogels were more resistant to digestion than the current product, fibrin sealant.

Usage of xan-GMA Hydrogels

Shear thinning is favored for the extrusion or injection-based application of hydrogels (Alarcin et al., 2018; Liu et al., 2018). As for xanthan alone, it is reported to be a special polysaccharide characterized by its high viscosity. More interestingly, xanthan's viscosity became lower after application of shear forces (Zhong et al., 2013), which is also known as shear thinning. Although modifications were carried out to xanthan,

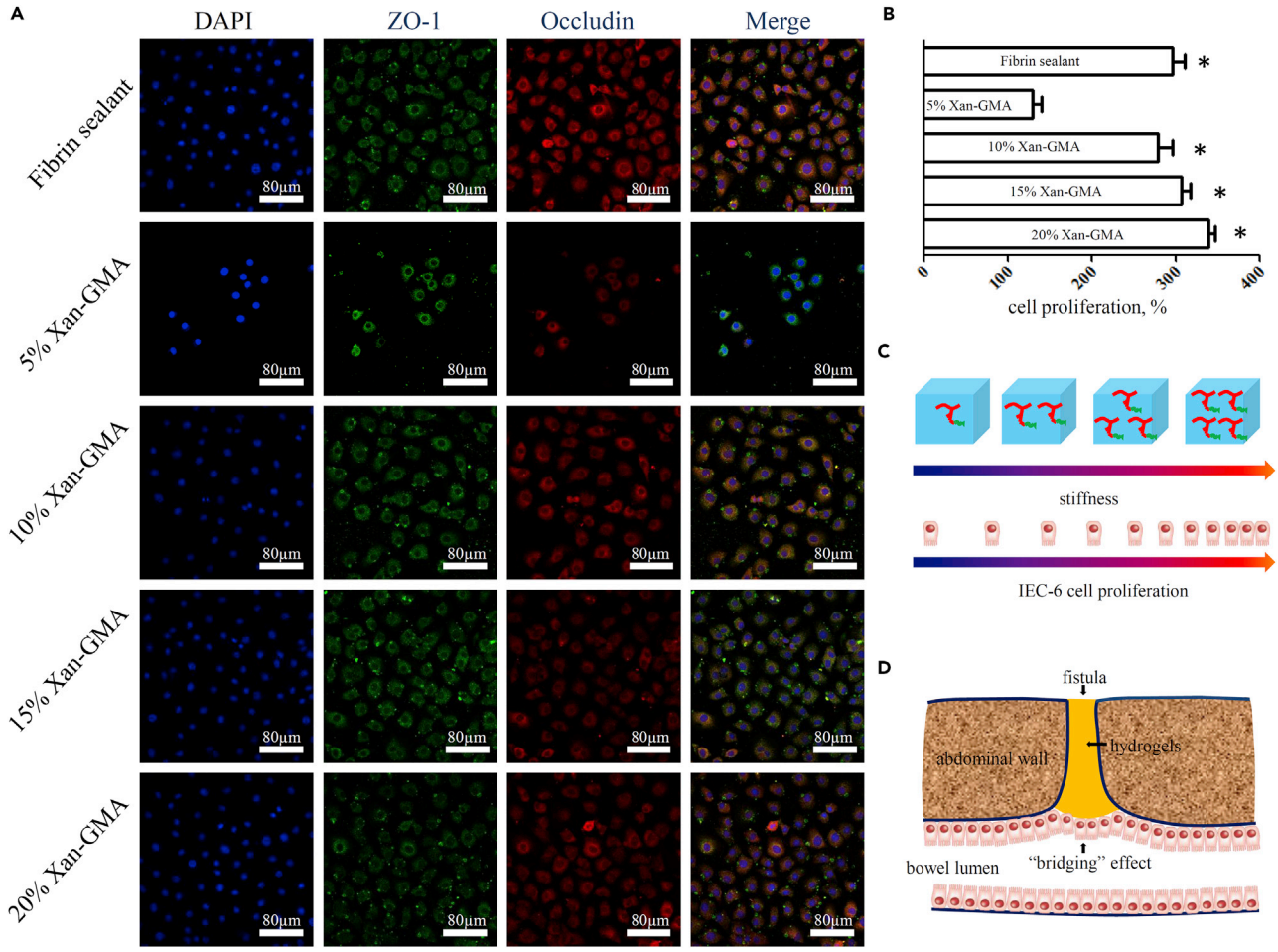

Figure 3. Response of IEC-6 Cells to xan-GMA Hydrogels

(A) Immunofluorescent staining of TJ proteins, ZO-1 and occludin.

(B) Proliferation ratio of IEC-6 cells, compared with 5% xan-GMA; *$p < 0.001$.

(C) Schematic diagram to demonstrate the rise of cell proliferation with improvement of hydrogel stiffness.

(D) Schematic diagram of the potential mechanism, the "bridging" effect for hydrogels to repair GI fistula.

the xan-GMA solution and hydrogels both showed shear-thinning behavior. As shown in Figures 5A–5D, negative linear relations of viscosity and shear rate were presented regardless of gelation. The high viscosity of xan-GMA solution in the static condition enabled adhesion of xan-GMA solution to the fistula during gelation, thus preventing disaggregation caused by GI fluids. Moreover, gelation further improved the viscosity because the molecular weight of xan-GMA was enlarged after photopolymerization.

To confirm the injectability, we injected 10% xan-GMA solution. As shown in Video S1, the logo of SEU was smoothly and accurately depicted through manual operation. After UV light exposure, this logo was gelated so that it could be lifted up (Figures 5E and 5F). These results validated that xan-GMA hydrogels could be injected during the management of GI fistula.

Strategy to Overcome Tissue Regeneration/Hydrogel Degradation Mismatch

The 10% xan-GMA hydrogels were degraded around 12% in the presence of IEC-6 cells within 8 days (the maximum duration of GI fistula healing) (Figure S5), which would become a hindrance at the late stage of fistula repair. However, hydrogels that were shrinkable by certain stimuli were easier to be removed, thus not acting as a foreign body in regenerating tissues, regardless of their degradation speed. Based on this concept, we explored the response of xan-GMA hydrogels to $CaCl_2$ solution by reference to current

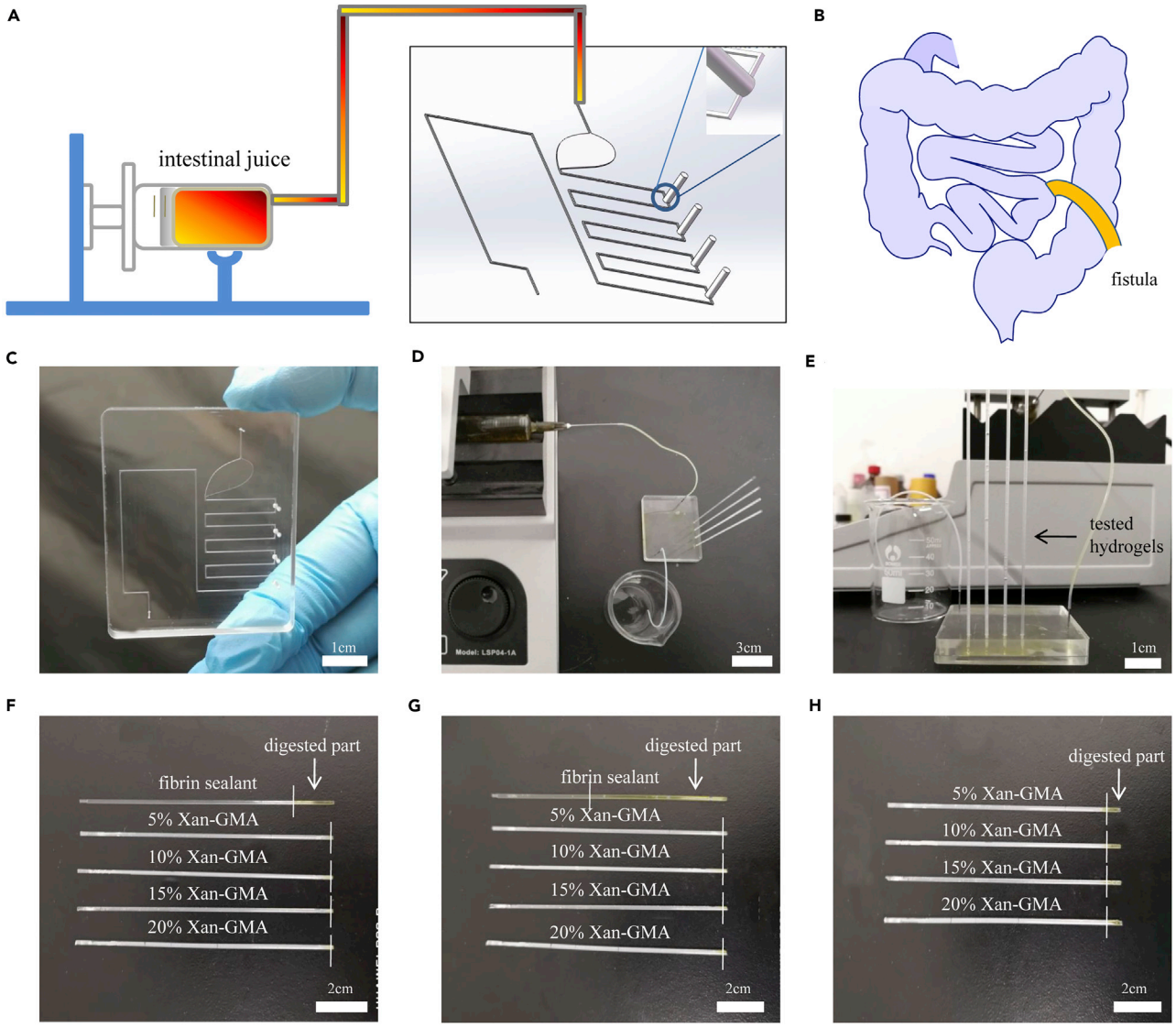

Figure 4. *Ex Vivo* Evaluation of Anti-digestive Performance Using a Simulated Gut Microfluidic Chip

(A) Schematic diagram of the detection device used for the measurement of anti-digestive abilities. The embedded picture in the black frame represents the STL file of the programmed microfluidic chip model.

(B) Schematic diagram of GI fistula.

(C) Appearance of the simulated gut microfluidic chip.

(D) Composition of the entire detection device.

(E) Real-time monitoring ability of the microdevice to detect the anti-digestive performance.

(F–H) Digestion results of tested hydrogels at (F) 2 hr, (G) 6 hr, and (H) 3 days, respectively.

literatures (Izawa et al., 2009, 2014). Through repeated immersion in $CaCl_2$ solutions, the xan-GMA hydrogels exhibited a reversible swelling-shrinking character (Figure 6A). The extent of swelling-shrinking behavior was magnified with the decrease in xan-GMA concentration, which was consistent with the aforementioned results for the swelling ratio. To explain further the underlying reasons, we used different concentrations of $CaCl_2$ solution (Figure 6B). The outcomes indicated that for 5% xan-GMA hydrogels, higher osmotic pressure caused by the increase of $CaCl_2$ concentration induced a more marked shrinking response. In addition, the conformation of xan-GMA was impaired in the presence of $CaCl_2$. The broad diffraction peak at 20° represented the double-helix conformation maintained by hydrogen bond interactions, and the addition of $CaCl_2$ led to its loss (Figure 6C). This was probably because the calcium ions had

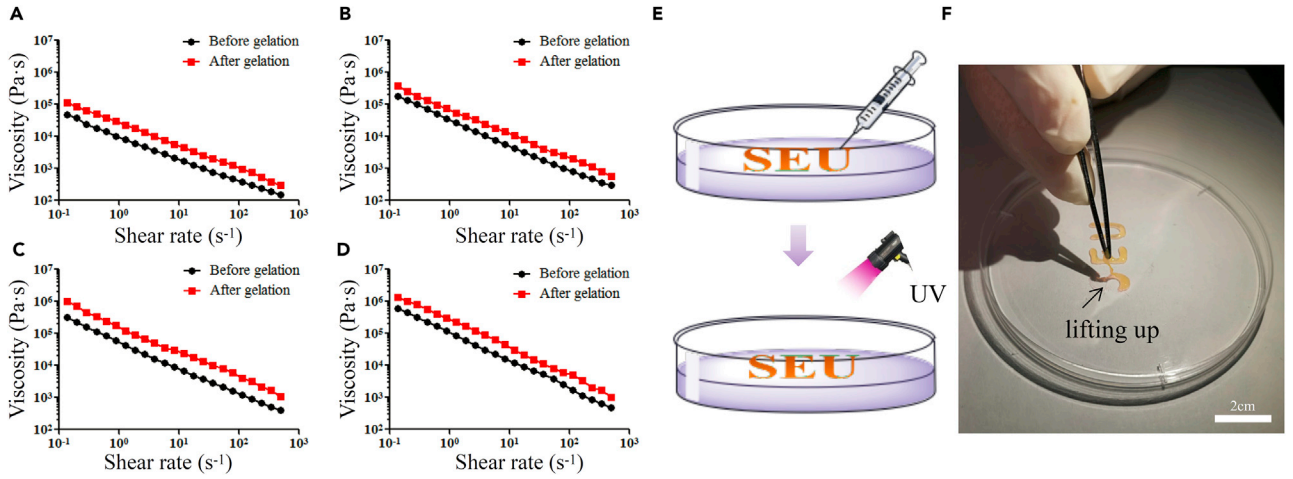

Figure 5. Injectability of xan-GMA Hydrogels in Practice

(A–D) Negative linear relations of viscosity and shear rate for xan-GMA solution and hydrogels at concentrations of (A) 5%, (B) 10%, (C) 15%, and (D) 20%, respectively.

(E) Schematic diagram of the process of hydrogel injection and photopolymerization.

(F) UV-induced solidification of the logo, SEU.

higher affinity to the carboxyl$^-$ groups of xan-GMA so that the original hydrogen bonds were interrupted. The emerging ionic cross-linking tightened the structure of the hydrogels to force water out. Therefore, changes in external osmotic pressure and internal conformation synergistically accounted for the observed swelling-shrinking performance (Figure 6D). This performance reduced the size of the injected hydrogel and removed it from the GI fistula at the appropriate time.

CONCLUSION

In this study, we introduced an anti-digestive hydrogel inspired from an enzyme-resistant dietary fiber, xanthan. This xan-GMA hydrogel showed great potential in closing GI fistula. First, it could be used through injection, allowing convenient application. In addition, this type of hydrogel displayed a high viscosity when free from external forces, which could contribute to tight adhesion of the hydrogel to the surrounding tissues for preventing intestinal juice leakage. Moreover, intestinal epithelial cells expressed the functional proteins (ZO-1 and occludin) to repair the fistula through the "bridging" effect, especially when cultured on a stiffer hydrogel surface. Furthermore, a practical method for removal of the hydrogel was given based on the swelling-shrinking behavior; therefore concern about hydrogel retention was relieved. Above all, our experiments provide strong evidence for xan-GMA hydrogels to achieve more satisfactory prognosis than the fibrin sealant in closing GI fistula, even though there is no specific animal model for further examinations. Our next step will directly focus on the clinical translational applications of this hydrogel based on a permitted clinical trial.

Limitations of Study

The xan-GMA hydrogels have not been tested *in vivo* due to the lack of a specific GI fistula animal model.

METHODS

All methods can be found in the accompanying Transparent Methods supplemental file.

DATA AND SOFTWARE AVAILABILITY

The authors provide detailed description of methods and original data upon request.

SUPPLEMENTAL INFORMATION

Supplemental Information includes Transparent Methods, five figures, and one video can be found with this article online at https://doi.org/10.1016/j.isci.2018.09.011.

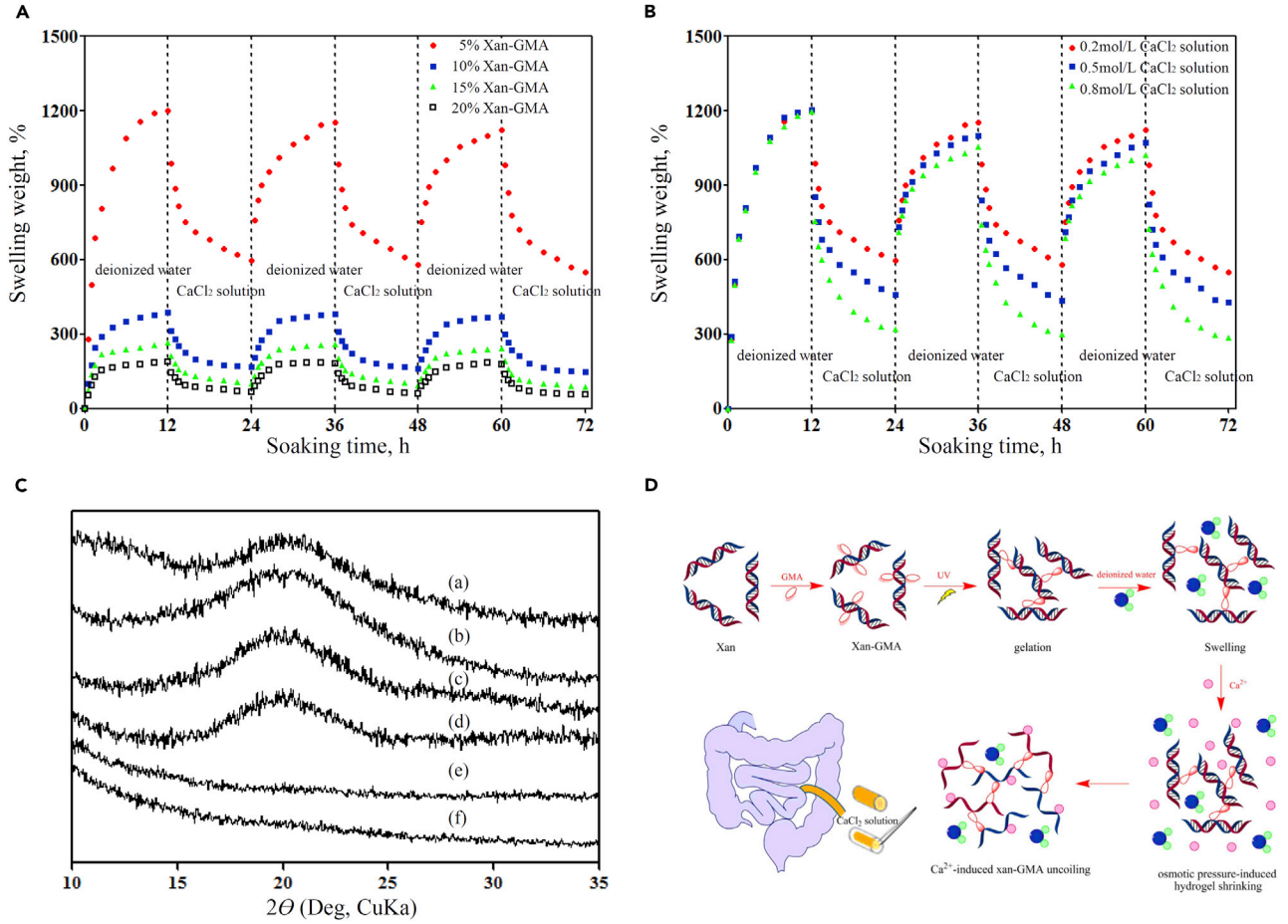

Figure 6. Prevention of the Improper Retention of xan-GMA Hydrogels Based on Their Swelling-Shrinking Behavior

(A) Repeated swelling-shrinking performance of xan-GMA hydrogels caused by $CaCl_2$ solution.

(B) Impacts of concentration of $CaCl_2$ solution on the swelling-shrinking activity.

(C) Conformational transition from the ordered double-stranded helix to the disordered form after immersion in $CaCl_2$ solution; the peak at 20° represented the double-helix conformation. a, Xanthan; b, xan-GMA; c, 5% xan-GMA hydrogel without $CaCl_2$; d, 20% xan-GMA hydrogel without $CaCl_2$; e, 5% xan-GMA hydrogel with $CaCl_2$; f, 20% xan-GMA hydrogel without $CaCl_2$.

(D) Schematic diagram for describing the specific reasons for the swelling-shrinking performance, i.e., osmotic pressure and conformational transition.

ACKNOWLEDGMENTS

We thank Fan Yang and Shuai Liu at the Nanjing Tech University for instructions regarding FTIR spectrophotometry, ^{1}H-NMR spectroscopy, and scanning electron microscopy. The study was supported by the Research funding of Nanjing Normal University (Grant no. 184080H202B135), Innovation Project of Military Medicine (Grant no. 16CXZ006), Key Project of Jiangsu Social Development (Grant no. BE2016752 and BE2017722) and National Major Scientific and Technological Special Project for "Significant New Drugs Development" (Grant no. 2018ZX09J18111-04).

AUTHOR CONTRIBUTIONS

J.H. and J.R. conceived and designed the experiments; J.H., Z.L., G.C., and Y.R. performed the experiments; J.H. and X.W. analyzed the data; J.R. and X.W. contributed reagents/materials/analysis tools; J.H. and Y.R. wrote the paper. J.H. and Q.H. revised this paper.

DECLARATION OF INTERESTS

We declare no potential conflicts of interest concerning the research, authorship, and/or publication of this article.

Received: July 24, 2018
Revised: August 29, 2018
Accepted: September 7, 2018
Published: October 26, 2018

REFERENCES

Alarcin, E., Lee, T.Y., Karuthedom, S., Mohammadi, M., Brennan, M.A., Lee, D.H., Marrella, A., Zhang, J., Syla, D., Zhang, Y.S., et al. (2018). Injectable shear-thinning hydrogels for delivering osteogenic and angiogenic cells and growth factors. Biomater. Sci. *6*, 1604–1615.

Altomare, D.F., Serio, G., Pannarale, O.C., Lupo, L., Palasciano, N., Memeo, V., and Rubino, M. (1990). Prediction of mortality by logistic regression analysis in patients with postoperative enterocutaneous fistulae. Br. J. Surg. *77*, 450–453.

Bitar, K.N., Raghavan, S., and Zakhem, E. (2014). Tissue engineering in the gut: developments in neuromusculature. Gastroenterology *146*, 1614–1624.

Bitar, K.N., and Zakhem, E. (2016). Bioengineering the gut: future prospects of regenerative medicine. Nat. Rev. Gastroenterol. Hepatol. *13*, 543–556.

Bueno, V.B., Takahashi, S.H., Catalani, L.H., de Torresi, S.I., and Petri, D.F. (2015). Biocompatible xanthan/polypyrrole scaffolds for tissue engineering. Mater. Sci. Eng. C Mater. Biol. Appl. *52*, 121–128.

Campos, A.C., Andrade, D.F., Campos, G.M., Matias, J.E., and Coelho, J.C. (1999). A multivariate model to determine prognostic factors in gastrointestinal fistulas. J. Am. Coll. Surg. *188*, 483–490.

Cruz-Acuna, R., Quiros, M., Farkas, A.E., Dedhia, P.H., Huang, S., Siuda, D., Garcia-Hernandez, V., Miller, A.J., Spence, J.R., Nusrat, A., et al. (2017). Synthetic hydrogels for human intestinal organoid generation and colonic wound repair. Nat. Cell Biol. *19*, 1326–1335.

de Vos, P., Lazarjani, H.A., Poncelet, D., and Faas, M.M. (2014). Polymers in cell encapsulation from an enveloped cell perspective. Adv. Drug Deliv. Rev. *67-68*, 15–34.

Elizalde-Pena, E.A., Zarate-Trivino, D.G., Nuno-Donlucas, S.M., Medina-Torres, L., Gough, J.E., Sanchez, I.C., Villasenor, F., and Luna-Barcenas, G. (2013). Synthesis and characterization of a hybrid (chitosan-g-glycidyl methacrylate)-xanthan hydrogel. J. Biomater. Sci. Polym. Ed. *24*, 1426–1442.

Ghobril, C., and Grinstaff, M.W. (2015). The chemistry and engineering of polymeric hydrogel adhesives for wound closure: a tutorial. Chem. Soc. Rev. *44*, 1820–1835.

Holzwarth, G., and Prestridge, E.B. (1977). Multistranded helix in xanthan polysaccharide. Science *197*, 757–759.

Huang, J., Deng, Y., Ren, J., Chen, G., Wang, G., Wang, F., and Wu, X. (2018). Novel in situ forming hydrogel based on xanthan and chitosan re-gelifying in liquids for local drug delivery. Carbohydr. Polym. *186*, 54–63.

Huang, J.J., Ren, J.A., Wang, G.F., Li, Z.A., Wu, X.W., Ren, H.J., and Liu, S. (2017). 3D-printed "fistula stent" designed for management of enterocutaneous fistula: an advanced strategy. World J. Gastroenterol. *23*, 7489–7494.

Izawa, H., Kaneko, Y., and Kadokawa, J. (2009). Unique gel of xanthan gum with ionic liquid and its conversion into high performance hydrogel. J. Mater. Chem. *19*, 6969.

Izawa, H., Nishino, S., Maeda, H., Morita, K., Ifuku, S., Morimoto, M., Saimoto, H., and Kadokawa, J. (2014). Mineralization of hydroxyapatite upon a unique xanthan gum hydrogel by an alternate soaking process. Carbohydr. Polym. *102*, 846–851.

Koetting, M.C., Guido, J.F., Gupta, M., Zhang, A., and Peppas, N.A. (2016). pH-responsive and enzymatically-responsive hydrogel microparticles for the oral delivery of therapeutic proteins: effects of protein size, crosslinking density, and hydrogel degradation on protein delivery. J. Control Release *221*, 18–25.

Korcz, E., Kerenyi, Z., and Varga, L. (2018). Dietary fibers, prebiotics, and exopolysaccharides produced by lactic acid bacteria: potential health benefits with special regard to cholesterol-lowering effects. Food Funct. *9*, 3057–3068.

Kumar, A., Deepak, Sharma, S., Srivastava, A., and Kumar, R. (2017). Synthesis of xanthan gum graft copolymer and its application for controlled release of highly water soluble Levofloxacin drug in aqueous medium. Carbohydr. Polym. *171*, 211–219.

Kumar, A., Rao, K.M., and Han, S.S. (2018). Application of xanthan gum as polysaccharide in tissue engineering: a review. Carbohydr. Polym. *180*, 128–144.

Li, H., Hou, W., and Li, X. (2012). Interaction between xanthan gum and cationic cellulose JR400 in aqueous solution. Carbohydr. Polym. *89*, 24–30.

Liu, K., Zang, S., Xue, R., Yang, J., Wang, L., Huang, J., and Yan, Y. (2018). Coordination-triggered hierarchical folate/zinc supramolecular hydrogels leading to printable biomaterials. ACS Appl. Mater. Interfaces *10*, 4530–4539.

Liu, S., Bastola, A.K., and Li, L. (2017). A 3D printable and mechanically robust hydrogel based on alginate and graphene oxide. ACS Appl. Mater. Interfaces *9*, 41473–41481.

Makhado, E., Pandey, S., Nomngongo, P.N., and Ramontja, J. (2017). Fast microwave-assisted green synthesis of xanthan gum grafted acrylic acid for enhanced methylene blue dye removal from aqueous solution. Carbohydr. Polym. *176*, 315–326.

Motealleh, A., and Kehr, N.S. (2017). Nanocomposite hydrogels and their applications in tissue engineering. Adv. Healthc. Mater. *6*, 1600938.

Reis, A.V., Fajardo, A.R., Schuquel, I.T., Guilherme, M.R., Vidotti, G.J., Rubira, A.F., and Muniz, E.C. (2009). Reaction of glycidyl methacrylate at the hydroxyl and carboxylic groups of poly(vinyl alcohol) and poly(acrylic acid): is this reaction mechanism still unclear? J. Org. Chem. *74*, 3750–3757.

Staruch, R.M., Glass, G.E., Rickard, R., Hettiaratchy, S.P., and Butler, P.E. (2017). Injectable pore-forming hydrogel scaffolds for complex wound tissue engineering: designing and controlling their porosity and mechanical properties. Tissue Eng. Part B Rev. *23*, 183–198.

Tseng, T.C., Tao, L., Hsieh, F.Y., Wei, Y., Chiu, I.M., and Hsu, S.H. (2015). An injectable, self-healing hydrogel to repair the central nervous system. Adv. Mater. *27*, 3518–3524.

Wu, X., Ren, J., Gu, G., Wang, G., Han, G., Zhou, B., Ren, H., Yao, M., Driver, V.R., and Li, J. (2014). Autologous platelet rich fibrin glue for sealing of low-output enterocutaneous fistulas: an observational cohort study. Surgery *155*, 434–441.

Xiao, B., Zhang, Z., Viennois, E., Kang, Y., Zhang, M., Han, M.K., Chen, J., and Merlin, D. (2016). Combination therapy for ulcerative colitis: orally targeted nanoparticles prevent mucosal damage and relieve inflammation. Theranostics *6*, 2250–2266.

Zhong, L., Oostrom, M., Truex, M.J., Vermeul, V.R., and Szecsody, J.E. (2013). Rheological behavior of xanthan gum solution related to shear thinning fluid delivery for subsurface remediation. J. Hazard. Mater. *244-245*, 160–170.

ISCI, Volume *8*

Supplemental Information

Bioinspired Anti-digestive Hydrogels Selected by a Simulated Gut Microfluidic Chip for Closing Gastrointestinal Fistula

Jinjian Huang, Zongan Li, Qiongyuan Hu, Guopu Chen, Yanhan Ren, Xiuwen Wu, and Jianan Ren

Supplemental information:

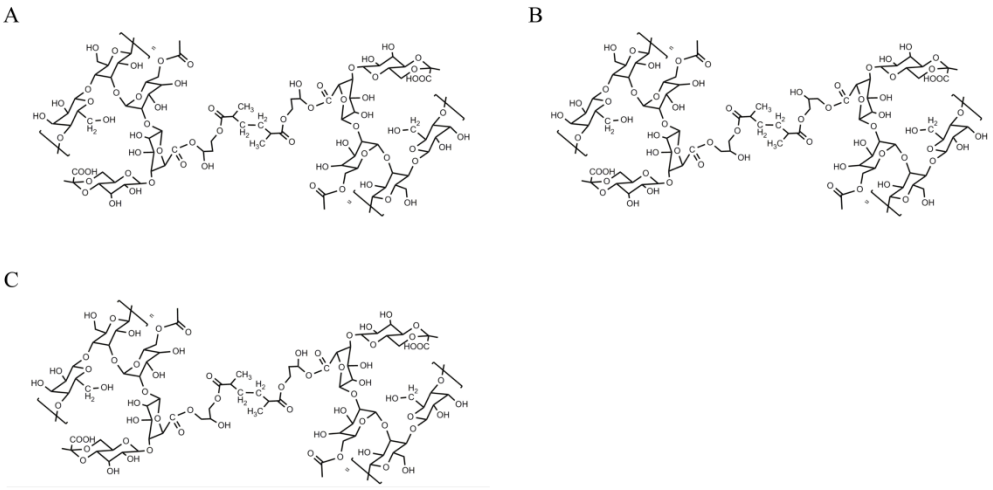

Figure S1, related to Figure 1A. (A-C) Three combinations of photopolymerized xan-GMA due to the presence of its isomers.

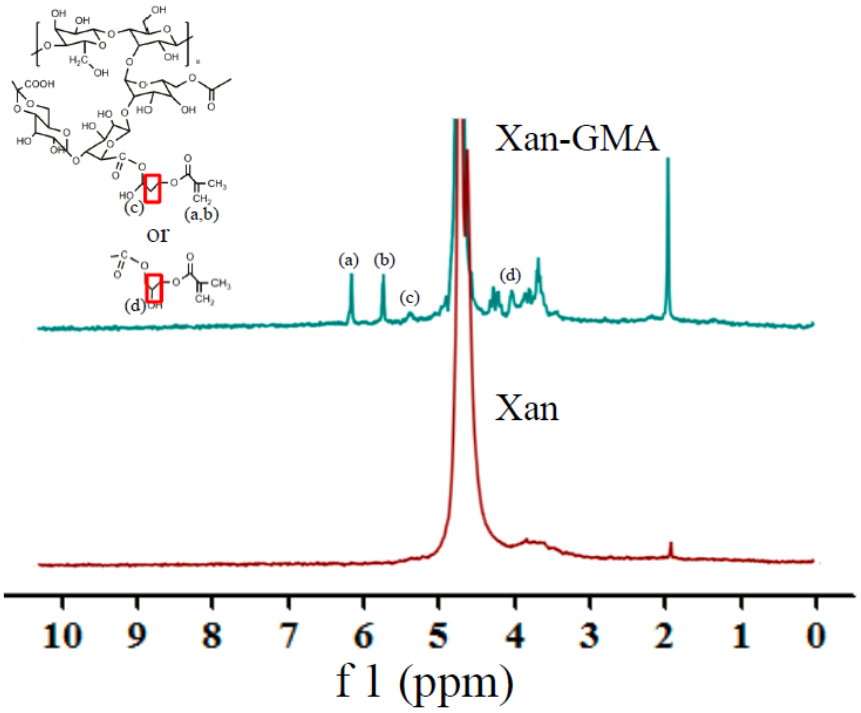

Figure S2, related to Figure 1B. The magnified version of Figure 1B regarding the ^{1}H-NMR spectrum, a=6.17, b=5.76, c=5.06 and d=4.02.

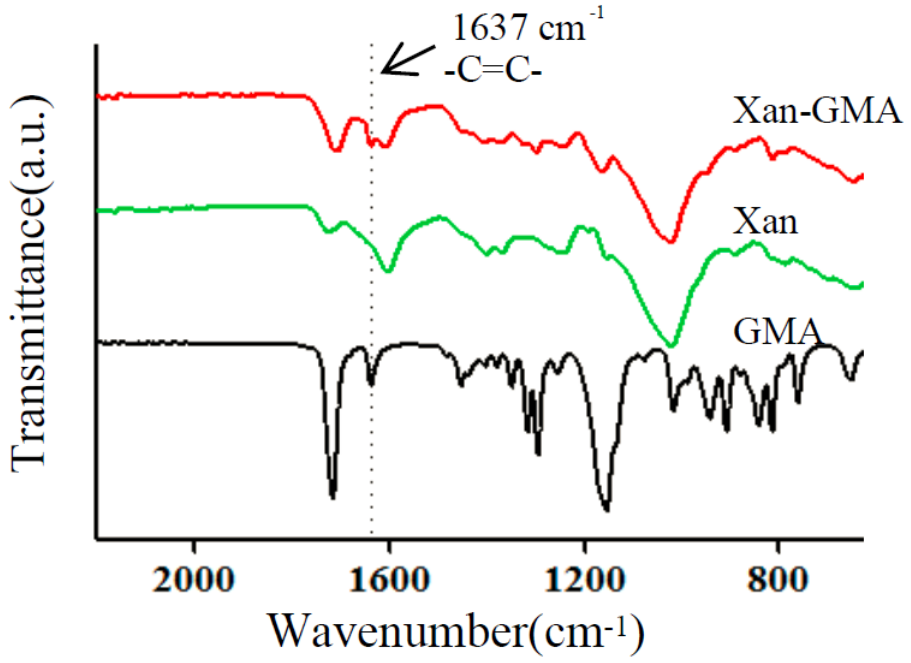

Figure S3, related to Figure 1C. The magnified version of Figure 1C regarding the FTIR spectrum, the peak at 1637cm^{-1} refers to the C=C groups in GMA.

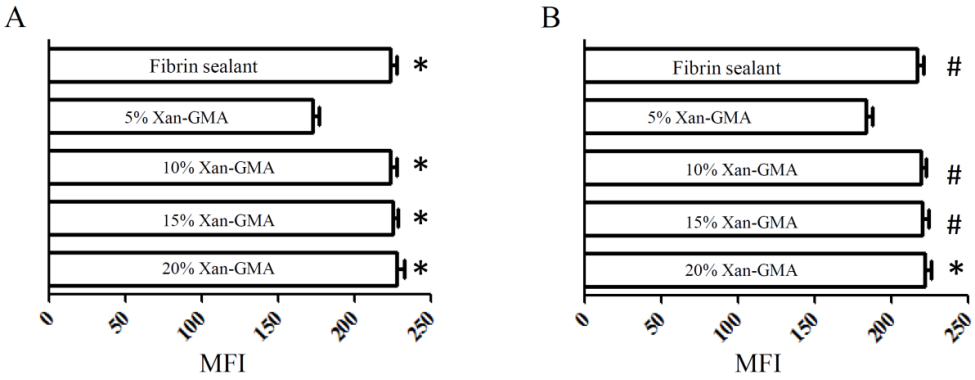

Figure S4, related to Figure 3A. Semiquantitative fluorescence intensity of TJ proteins using Image J software. (A) Occludin-1, compared with 5% xan-GMA, $^{*}P$<0.001. (B) ZO-1, compared with 5% xan-GMA, $^{\#}P$<0.01, $^{*}P$<0.001, MFI: mean fluorescence intensity.

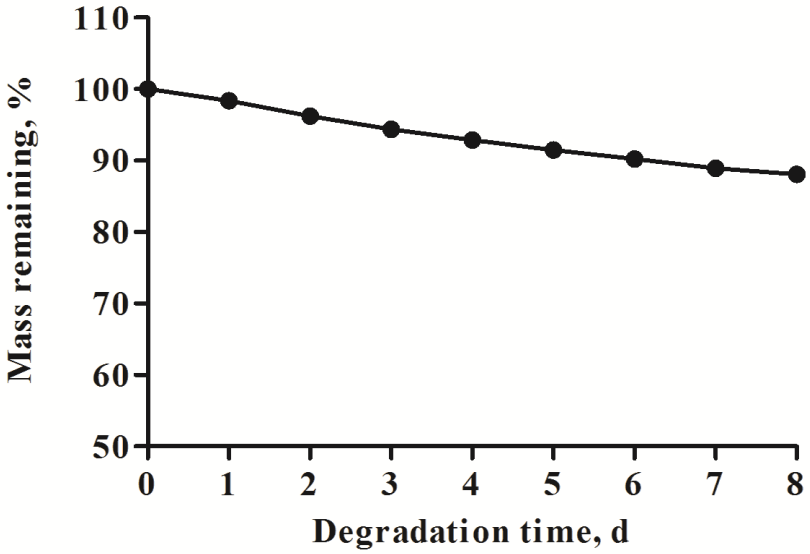

Figure S5, related to Figure 6. The degradation behavior of the 10% xan-GMA hydrogels in the presence of IEC-6 cells, indicating the xan-GMA hydrogels would become a hindrance at the late stage of fistula repair if not removed.

Transparent Methods:

1. Materials

Xanthan gum (viscosity of 1% aqueous solution at 20°C: 1450-2000 mPa.s, TCI Development Co. Ltd, Shanghai, China); GMA (Aladdin®, Shanghai, China); hydrochloric acid (36-38wt%, Jiuyi Reagent Co. Ltd, Shanghai, China); 2-hydroxy-4'-(2-hydroxyethoxy) -2-methylpropiophenone (I-2959, Sigma-Aldrich®, St. Louis, MO, USA); polydimethylsiloxane (PDMS, generated from the liquid silicon elastomers A and B liquid mixing at a volume ratio of 10 : 1, silicon elastomer was purchased from Dow Corning Corp, Midland, Michigan, USA); uncontaminated intestinal juice (obtained from a patient with duodenal fistula, amylase was quantified as 20000 U/L using a dry chemistry method in the laboratory department of Jinling Hospital). All other reagents were of analytical reagent grade.

2. Synthesis of xan-GMA

The protocol of xan-GMA synthesis was first established. First, 0.6% (w/v) xanthan aqueous solution was prepared by dissolving xanthan powders into deionized water, followed by stirring overnight. Then, 270 mL of such solution was poured into a round-bottom flask and heated to 80 °C using an oil bath (model: DF-101S, Xinbao Instrument Co. Ltd, Dongguan, China). Afterwards, hydrochloric acid was used to adjust its pH to 4.2-4.8, and 1.88 mL of GMA was added dropwise. After 12 h of reaction at 80 °C, the resultant solution was collected and then dialyzed for 3 d using dialysis membranes (molecular weight cut-off: 12-14 kDa) to remove unreacted residues. Finally, the solution was lyophilized in a freeze dryer (Xiongdi Instrument Co. Ltd, Zhengzhou, China) and stored in a sealed bag at 4 °C.

3. Synthesis of xan-GMA hydrogels

Xan-GMA was dissolved in deionized water containing 0.1% (w/v) I-2959 to obtain solutions with different concentrations at 5% (w/v), 10% (w/v), 15% (w/v) and 20% (w/v). Gelation of xan-GMA solution was initiated under UV-light exposure (365 nm, ~6.0 W/cm^2, model: UVPL-411, Yunhe Tech Co. Ltd, Suzhou, China) for 40s.

4. Confirmation of GMA conjugation to xanthan

4.1 Fourier-transform infrared (FTIR) spectrometry. An FTIR spectrophotometer was

applied to investigate the FTIR spectra of GMA, xanthan and xan-GMA using a Nicolet-6700 spectrometer (Thermo®, USA) at room temperature, in the wave number range of 4000–500 cm^{-1} using the KBr pellet technique. The liquids or powders were ground to a dry KBr disk and 32 scans at a resolution of 4 cm^{-1} were used to record the spectra.

4.2 NMR spectrum detection. Xanthan and xan-GMA were dissolved in deuterated solvents. The modification of xanthan and the purity of xan-GMA in final products were characterized by ^{1}H NMR (Bruker 500, Germany).

5. Morphology

The porosity of hydrogels that mimics the extracellular matrix can support cell growth and tissue regeneration. This structure was observed under a scanning electron microscope (SEM; model: S-4800, Hitachi®, Japan). Specifically, the xan-GMA hydrogels with varied xan-GMA concentrations were freeze-dried and their vertical sections were imaged after coating with a thin layer of gold.

6. Swelling ratio

The swelling ratio of xan-GMA hydrogels was determined by the following formula (Ghobril and Grinstaff, 2015):

$$\text{Swelling ratio} = (M_{\text{swollen gel}} - M_{\text{dried gel}}) / M_{\text{dried gel}}$$

$M_{\text{dried gel}}$ and $M_{\text{swollen gel}}$ stand for the mass of dried hydrogel and swollen hydrogel at equilibrium, respectively. Specifically, tested hydrogels were immersed in phosphate-buffered saline (PBS). At each preset time, they were removed, and the surface moisture was immediately wiped off using tissue paper. After the hydrogels were weighed, they were returned to the PBS buffer. This process was repeated until equilibrium was attained. To confirm that the swelling ratio was changed with xan-GMA concentration, the correlation of swelling ratio and pore density per visual field at 50× magnification was described using Graphpad Prism 5 software.

7. Rheometry

Rheological properties of the hydrogels were characterized using a rheometer (model: MCR302, Anton Paar Co. Ltd, Austria) with the parallel plates at a gap size of 1mm. In the oscillatory strain sweep experiment, the constant frequency was fixed at 10 Hz,

while in the oscillatory frequency sweep experiment, the constant strain was fixed at 1%. For the oscillatory time sweep experiment, an external UV-light with three on-and-off cycles was applied to the hydrogels with the constant strain at 1% and frequency at 10 Hz.

8. Injectability

This injectability of xan-GMA hydrogels was also tested using the rheometer. The steady state shear flow was from 0.1 to 500s^{-1} of shear rate. Additionally, the practice of injection was performed on the 10% xan-GMA solution by handwriting the logo of Southeast University, SEU. To make the logo clearer, the dye of rhodamine 123 (Aladdin®, Shanghai, China) was added to the solution.

9. Swelling-shrinking property

The role of $CaCl_2$ on the shrinking of xan-GMA hydrogels was investigated as follows. First, tested hydrogels were immersed in deionized water and weighed at each preset time until the weight tended to be stable. Later, they were moved into 0.2mol/L $CaCl_2$ solution and weighed at each preset time until the weight became stable. The entire process was repeated three times. In addition, the concentration of $CaCl_2$ solution was changed to 0.5 mol/L or 0.8 mol/L to study the influence of the concentration on the shrinking ability of the hydrogels. Moreover, the conformation of the hydrogels in deionized water or 0.2 mol/L $CaCl_2$ solution was studied using the XRD assay (model: XD-3A, Shimadzu®, Japan).

10. Anti-digestive property

The anti-digestive performance was detected using a simulated gut microfludic chip. This chip was tailor-made through a series of processes including model code programming, 3D wax jetting, PDMS replicating, wax dissolving and PDMS-to-glass bonding (Li et al., 2017). The chip could mimic the anatomy of GI fistula. At the "fistula sites", we examined the anti-digestive property of the tested gels. Specifically, the fibrin sealant and the xan-GMA hydrogels were gelated in glass capillaries (~100 μm in diameter, Changcheng Instrument Co. Ltd, Shanghai, China), followed by insertion at the "fistula sites". The intestinal juice was pumped at 37°C at 0.2mL/h using a syringe pump (model: LSP04-1A, LongerPump®, China). The anti-digestive

property was evaluated by the ratio of digested part to the full-length.

11. Maintenance of gut barrier functions

The functions of IEC-6 cells (KeyGEN®, Nanjing, China) were studied by cell culture on the hydrogel surface. Specifically, the fibrin sealant and xan-GMA hydrogels were injected at the bottom of confocal dishes (thickness: ~1mm) and gelated by UV-light exposure. After washing twice using PBS, 1 mL of 5×10^5/mL IEC-6 cells were added in the dishes and cultured in a cell incubator. Three days later, IEC-6 cells were fixed with 4% (w/v) paraformaldehyde for 30 min at room temperature, and then proceeded to 0.05% (w/v) Triton X-100 for permeabilization. For immunofluorescent analysis of tight junction (TJ) proteins, we labeled the cells with ZO-1 antibody conjugated with FITC (green) (ab150266, Abcam®, USA) diluted at 1/20 and occludin antibody (sc-8145, Santa®, USA) using 1/100 dilution, followed by the donkey anti-goat IgG (ab150130, Alexa Fluor555®, USA) secondary antibody at 1/1000 dilution (red). The nuclear counter stain was DAPI (blue). A confocal scanning microscope (model: FV1000, Olympus®, Tokyo, Japan) was used for image analysis. Moreover, proliferation of IEC-6 cells on the hydrogel surface was detected using MTT assay. Similarly, the fibrin sealant and xan-GMA hydrogels were gelated at the bottom of a 96-well plate (thickness: ~1mm). 100μL of 2×10^4/mL IEC-6 cells were added to the wells, followed by adding 100μL Dulbecco's modified Eagle's medium. After incubation for 72 h, 20 μL of MTT (5 mg/mL) was added to each well and further incubated for 4 h. Formazan salt was dissolved in 200μL DMSO. After it was thoroughly dissolved, the resultant solution was transferred to another 96-well plate and measured with a microplate spectrophotometer (BioTek Instrument Co. Ltd, USA) at 570 nm. Each sample was replicated in three wells.

12. Degradation behavior of the hydrogel in the presence of IEC-6 cells

The 10% xan-GMA hydrogels in a 24-well plate were weighed at equilibrium (Wi), where the weight of the swollen hydrogels in the cell culture media of DMEM (KeyGEN®, Nanjing, China) is steady. Then, 1 mL of 5×10^5/mL IEC-6 cells were added in each well. At different time points, we removed the media of the specific wells and weighed the hydrogels (Wd). Meanwhile, we also re-introduced the fresh

media to the rest of the wells. The weight remaining percentage (Wr) of the hydrogel was calculated as follows (Ghobril and Grinstaff, 2015):

$$Wr = Wd / Wi \times 100\%.$$

References:

Ghobril, C., and Grinstaff, M.W. (2015). The chemistry and engineering of polymeric hydrogel adhesives for wound closure: a tutorial. CHEM SOC REV *44*, 1820-1835.

Li, Z., Yang, J., Li, K., Zhu, L., and Tang, W. (2017). Fabrication of PDMS microfluidic devices with 3D wax jetting. RSC ADV *7*, 3313-3320.